# Computational method for multidimensional quantal dynamics of polynomially interacting oscillator systems

T. Okushima*
*Department of Physics, Tokyo Metropolitan University, Minami-Ohsawa, Hachioji, Tokyo 192-0397, Japan*
(Received 11 January 2004; published 21 July 2004)

We propose a numerical algorithm for computing quantal dynamics, which is tailored for a generic multidimensional model of low-energy dynamics, i.e., polynomially interacting oscillator system. This algorithm evaluates symplectic integrators effectively, by using block tridiagonality of the interaction operator, and thus accurately preserves unitarity with time. A practical advantage of this method is that high-order integrators are easily implemented even for time-dependent parameter systems. We demonstrate the accuracy and usefulness by applying it to a $\phi^4$ model.

DOI: 10.1103/PhysRevE.70.016705 PACS number(s): 02.70.Bf, 31.15.Fx, 02.60.−x

## I. INTRODUCTION

Multidimensional quantal dynamics of nonintegrable systems is a subject of recent intense interest because experimental technologies have opened the way for producing molecular Bose-Einstein condensates [1] and probing the dynamics of molecular motion on the time scale of vibrational and rotational periods [2,3]. Elucidation of the multidimensional dynamics will provide a more sound basis of controlling these atomic and molecular motions.

For computing the dynamics of these nonintegrable systems, a number of numerical methods have been developed, which are classified roughly into three methods: the recursive residue generation method (RRGM) [4,5], the Chebyshev method [5,6], and the symplectic integrator (SI) method (also referred to as the exponential product method) [7–9]. The RRGM permits multidimensional computation of transition probabilities for systems that are isolated or perturbed by monochromatic external fields. The Chebyshev method is a sophisticated algorithm, especially suitable for multidimensional systems [5]. However, the full advantage of the method is not taken for time-*dependent* parameter systems [10]. The SI method, which is a higher order generalization of split operator method, has an advantage of being applicable to time-dependent systems as easily as to time-independent systems, over the other methods. Being optimized with the use of fast Fourier transform (FFT) [5], the resulting SI-FFT method is proved to be extremely valuable for low-dimensional systems [10]. Unfortunately, this method is generally not practical for systems with more than three degrees of freedom, due to the storage and execution-time limitations.

In this paper, we develop a simple algorithm based on the SI method, which is tailored for a polynomially interacting oscillators system (PIOS). In Sec. II, the PIOS model is introduced as a generic model of multidimensional low-energy dynamics. An example of PIOS, a $\phi^4$ model, is also presented with the renormalization procedure. In Sec. III, we present our algorithm to evaluate the SI of PIOS with estimating its required storage and computational costs. In Sec. IV, the accuracy of our method is illustrated with the numerical application to the $\phi^4$ model. In Sec. V, we present our conclusion with remark on the application of our method to eigen-energy problem.

## II. PIOS AS A MODEL OF LOW-ENERGY DYNAMICS

### A. Introduction of PIOS

We introduce a PIOS, which describes low energy dynamics of multidimensional quantal dynamics.

Let us first consider an $N$-dimensional boson system with a normalized ground state. The Hamiltonian is expanded around the ground state

$$H = \sum_{j=1}^{N} \hbar\omega_j\left(n_j + \tfrac{1}{2}\right) + \sum_{q=3}^{\infty} V_q,$$

$$V_q = \sum_{\mathcal{O}(\ell^+,\ell^-)=q} W_{\ell^+,\ell^-} \prod_{j=1}^{N} (a_j^\dagger)^{\ell_j^+} (a_j)^{\ell_j^-}, \tag{1}$$

where $a_j$, $a_j^\dagger$, and $n_j$ ($\equiv a_j^\dagger a_j$) are the annihilation, creation, and number operators of $j$th mode with frequency $\omega_j$. They satisfy the commutation relations $[a_j, a_k^\dagger] \equiv a_j a_k^\dagger - a_k^\dagger a_j = \delta_{j,k}$. $V_q$ is the $q$th order part of the normal ordered interaction potential with $\ell^\pm = (\ell_1^\pm, \ell_2^\pm, \ldots, \ell_N^\pm)$, $\ell_j^\pm \geqslant 0$, and $\mathcal{O}(\ell^+,\ell^-) = \Sigma_j(\ell_j^+ + \ell_j^-)$. The coefficients $W_{\ell^+,\ell^-}$ satisfy the reality conditions $W_{\ell^+,\ell^-} = W^*_{\ell^-,\ell^+}$, where $W^*$ denotes the complex conjugate of $W$. Note that state $|0\rangle$, satisfying $a_j|0\rangle = 0$ for all $j$, is the mean field approximation of the true ground state and that number states created by $a_j^\dagger$ are good approximations for sufficiently low-lying eigenstates.

We now truncate the interaction terms $V_q$ at a finite order, since lower-order terms are generally more relevant for low-energy dynamics. For the truncated dynamics to mimic the original dynamics of Eq. (1), the maximum order $q_{\max}$ should be even, or quantum tunneling process would destroy $|0\rangle$ into lower energy, large amplitude states $\langle a_j\rangle \gg 1$, and thus the assumed ground state would become a metastable state. In the following only PIOS models with stable ground states are considered ($q_{\max}$= an even number).

The PIOS model includes paradigmatic dynamical models. For example, Fermi-Pasta-Ulam (FPU) $\beta$ and lattice $\phi^4$

*Electronic address: okushima@comp.metro-u.ac.jp

 

models are included in the fourth order PIOS ($q_{\max}=4$). Additionally, it effectively describes a wide range of physical phenomena, such as intramolecular vibrational redistribution [2,3,11,12], influence of Fermi resonance [13], and Bose-Einstein condensation dynamics [14,1].

From the standpoint of quantum-classical correspondence, the classical limit of a PIOS model generally belongs to a generic class of dynamical systems, i.e., moderately chaotic dynamical systems, which have wandering motions from fully chaotic to quasi-integrable regular motions and vice versa [15]. The quantal PIOS model is therefore a generic, quantum chaotic model. Moreover, the generosity is intrinsic because it is induced by underlying classical dynamics, in contrast to random matrix quantum chaotic models that contain random system parameters.

PIOS provides a unified frame in which multidimensional peculiarities in nonlinear dynamics are contained. This also leads a practical advantage of sharing programs between specific PIOS problems.

### B. $\phi^4$ model truncated in reciprocal space

Let us derive another PIOS model, $\phi^4$ model truncated in *reciprocal* space ($\phi^4$ MTRS), by truncating high frequency modes in $\phi^4$ self-interacting quantum field. First, using a real scalar field $\phi(x,t)$ and its conjugate field $\pi(x,t)$, the Hamiltonian of $\phi^4$ self-interacting field is given by

$$H \equiv \int_L dx(\pi\dot{\phi} - \mathcal{L}) = \int_L dx\left[\frac{1}{2}(\pi^2 + \phi'^2 + m^2\phi^2) + \frac{\lambda}{4!}\phi^4\right], \tag{2}$$

where the system is put in a one-dimensional box of length $L$. To quantize this system, we set the canonical commutation relation between the conjugate valuables

$$[\phi(x,t), \pi(y,t)] = i\hbar\delta(x-y),$$

$$[\phi(x,t), \phi(y,t)] = [\pi(x,t), \pi(y,t)] = 0, \tag{3}$$

where $\hbar$ is Planck's constant over $2\pi$.

Next, by setting the periodic boundary condition on the box, mode valuables $q_j, p_j$ ($j=\ldots-2,-1,0,1,2,\ldots$) are introduced in reciprocal space

$$q_j(t) = \int_L dx \frac{e^{-ik_j x}}{\sqrt{L}}\phi(x,t), \quad p_j(t) = \int_L dx \frac{e^{ik_j x}}{\sqrt{L}}\pi(x,t), \tag{4}$$

where $k_j \equiv 2\pi j/L$ is the wave number of $j$th mode. These $q_j, p_j$ satisfy the reality condition $q_{-j}=q_j^\dagger, p_{-j}=p_j^\dagger$ and the commutation relations $[q_j,q_l]=[p_j,p_l]=0$ and $[q_j,p_l]=i\hbar\,\delta_{j,l}$.

Here we just keep low frequency modes $j=0,\pm1,\pm2,\pm3,\ldots,\pm\Lambda$, where positive integer $\Lambda$ is a cutoff parameter, and truncate other higher frequency modes. The resulting $(2\Lambda+1)$ degrees of freedom oscillator system has the following Hamiltonian:

$$H = \sum_{j=-\Lambda}^{\Lambda} \frac{\hbar\omega_j}{2}(a_j^\dagger a_j + a_j a_j^\dagger) + \frac{\lambda\hbar^2}{4!\,L}\sum_{j_1,j_2,j_3,j_4=-\Lambda}^{\Lambda} \frac{\delta_{j_1+j_2+j_3+j_4,0}}{2\sqrt{\omega_{j_1}\omega_{j_2}\omega_{j_3}\omega_{j_4}}} \times (a_{j_1} + a_{-j_1}^\dagger)(a_{j_2} + a_{-j_2}^\dagger)(a_{j_3} + a_{-j_3}^\dagger)(a_{j_4} + a_{-j_4}^\dagger), \tag{5}$$

where annihilation and creation operators $a_j$, $a_j^\dagger$ are defined by

$$a_j \equiv \frac{1}{\sqrt{2}}(\tilde{q}_j + i\tilde{p}_{-j}), \quad a_j^\dagger \equiv \frac{1}{\sqrt{2}}(\tilde{q}_{-j} - i\tilde{p}_j), \tag{6}$$

with $j$th mode harmonic frequency $\omega_j=\sqrt{k_j^2+m^2}\equiv\omega(k_j)$ and the rescaled mode variables $\tilde{q}_j \equiv (\hbar/\omega_j)^{1/2}q_j, \tilde{p}_j \equiv (\hbar\omega_j)^{1/2}p_j$.

Note that compared to other lattice regularization model, such as FPU-$\beta$, lattice $\phi^4$ models, our finite dimensional model has fewer expansion terms of interaction part. As we see later in Sec. III, this fewer expansion terms improve the efficiency of our numerical algorithm. Hence, this model is a good model that can be efficiently evaluated with our method.

Due to the noncommutability between $a_j$ and $a_j^\dagger$, however, the normal ordered form of Hamiltonian (5) has squeezing terms, which shows that it is not a PIOS Hamiltonian (1), as it is. In order to elucidate this, setting $V$ as

$$V = \sum_{j_1,j_2,j_3,j_4=-\Lambda}^{\Lambda} \frac{\delta_{j_1+j_2+j_3+j_4,0}}{2\sqrt{\omega_{j_1}\omega_{j_2}\omega_{j_3}\omega_{j_4}}}(a_{j_1} + a_{-j_1}^\dagger)(a_{j_2} + a_{-j_2}^\dagger) \times (a_{j_3} + a_{-j_3}^\dagger)(a_{j_4} + a_{-j_4}^\dagger), \tag{7}$$

then we expand it and classify the monomials into zeroth, second, and fourth order polynomials of $V_0, V_2$, and $V_4$, respectively:

$$V_0 = 3\sum_{j_1,j_2} W_{j_1,j_1,j_2,j_2}, \tag{8}$$

$$V_2 = \sum_j 12\left(\sum_{j'} W_{j,j,j',j'}\right)n_j + \sum_{j\geqslant 1} 12\left(\sum_{j'} W_{j,j,j',j'}\right)(a_j a_{-j} + \text{H. c.}) \tag{9}$$

$$V_4 = :V:, \tag{10}$$

where $W_{j_1,j_2,j_3,j_4}=1/(2\sqrt{\omega_{j_1}\omega_{j_2}\omega_{j_3}\omega_{j_4}})$ and $:V:$ is the normal ordering of $V$.

Let us now derive a PIOS Hamiltonian by applying a basic renormalization procedure to Eq. (5). Assuming that $\omega_R(k)$ is the observed, renormalized frequency of wave number $k$ that is different from bare frequency $\omega(k)$ [16], we substitute $\omega^2(k)=\omega_R^2(k)-\delta\omega^2(k)$ for (5). Using the renormalized annihilation and creation operators, $a_j^R, a_j^{R\dagger}$, defined by

$$a_j^R \equiv \frac{1}{\sqrt{2}}(\tilde{q}_j^R + i\tilde{p}_{-k}^R), \quad a_j^{R\dagger} \equiv \frac{1}{\sqrt{2}}(\tilde{q}_{-k}^R - i\tilde{p}_k^R) \tag{11}$$

with $\tilde{q}_j^R \equiv [\hbar/\omega_R(k_j)]^{1/2}q_j$, $\tilde{p}_j^R \equiv [\hbar\omega_R(k_j)]^{1/2}p_j$, the Hamiltonian is expressed by

$$H = H^R + V_c, \tag{12}$$

where $H^R$ is an operator of the same form (5) with the replacement of $\omega(k), a_j$ with $\omega_R(k), a_j^R$, respectively, and

$$V_c = -\sum_j \frac{\delta\omega^2(k_j)}{2}\frac{\hbar}{2\omega_R(k_j)}(a_j^R a_{-j}^R + a_j^{R\dagger} a_{-j}^{R\dagger}) - \sum_k \frac{\delta\omega^2(k_j)}{2}\frac{\hbar}{2\omega_R(k_j)} 2a_j^{R\dagger} a_j^R - \sum_j \frac{\delta\omega^2(k_j)}{2}\frac{\hbar}{2\omega_R(k_j)} \tag{13}$$

The condition that $V_c$ cancels the squeezing operators in (12) is

$$\frac{\delta\omega^2(k_j)}{2}\frac{\hbar}{2\omega_R(k_j)} = \frac{\lambda}{4!}6\sum_{j'} W^R_{j,j,j',j'}, \tag{14}$$

which leads

$$\delta\omega^2(k) = \frac{\lambda\hbar}{4}\sum_{j'}\frac{1}{\omega_R(k_{j'})}. \tag{15}$$

This $k$-independent renormalization is equivalent to the mass renormalization $\delta\omega^2(k) = \delta m^2$. In addition to this, the mass renormalization simultaneously cancels all terms in $V_0$, and $V_2$. Thus, we have confirmed that the renormalized Hamiltonian has a PIOS form of

$$H = H_0^R + \frac{\lambda}{4\,!\,L}V_4^R. \tag{16}$$

In the following, we refer to this PIOS Hamiltonian as $\phi^4$ MTRS and drop the suffixes $R$ in (16) for notational simplicity.

## III. NUMERICAL METHOD

In this section, we develop a computational method for multidimensional PIOS dynamics.

After recalling the properties of SI that is required for our development, we give a truncation scheme that provides approximate, finite-dimensional quantum state spaces where wave functions are represented. Then a method for estimating SI on the truncated spaces is developed with estimation of computational time requirement.

### A. SI

The SI scheme for quantum time evolution has the theoretical advantage of preserving time reversal symmetry and unitarity, and the practical advantage that programing higher order SI is just several calls of second order SI $(SI)_2$ subroutines [7]. These merits are extended to time-dependent parameter systems in [8]. We here collect these useful results, without proof.

#### *1. Second order SI*

First, for a time-independent Hamiltonian $H$, the time evolution operator $U(\Delta t)$, with a small time step $\Delta t$, is given by

$$U(\Delta t) = \exp\left(-\frac{i\Delta t}{\hbar}H\right). \tag{17}$$

If $H$ is the sum of two operators, $H=A+B$, the associated second order SI, $S_2(\Delta t)$ $[=U(\Delta t)+O(\Delta t^3)]$, is given by a product of exponentials of $A$ and $B$:

$$S_2(\Delta t) \equiv e^{-(i\Delta t/2\hbar)A} e^{-(i\Delta t/\hbar)B} e^{-(i\Delta t/2\hbar)A}, \tag{18}$$

which satisfies the following time-reversibility and unitarity conditions:

$$S_2(-t) = S_2(t)^{-1}, \tag{19}$$

$$= S_2(t)^{\dagger}. \tag{20}$$

Note that, only when the operations of exponentials of $A$ and $B$ to any wave function are efficiently computable, as $H = T(p) + V(q)$ with the SI-FFT method, Eq. (18) becomes a practically useful expression.

Assuming operations of exponentials of $A_i (i=0,\ldots,r)$ are efficiently computable, the second order SI for

$$H = A_0 + A_1 + A_2 + \cdots + A_r \tag{21}$$

is given by

$$S_2(\Delta t) = e^{(x/2)A_r} e^{(x/2)A_{r-1}} e^{(x/2)A_{r-2}} \cdots e^{(x/2)A_1} e^{xA_0} \times e^{(x/2)A_1} \cdots e^{(x/2)A_{r-2}} e^{(x/2)A_{r-1}} e^{(x/2)A_r}, \equiv F_2^{(r)}(x) \tag{22}$$

where $x = i\Delta t/\hbar$.

#### *2. Higher order SI*

After Ref. [8], we here give a formal solution of fourth and sixth order symmetric SI that are composed of several $SI_2$ operations.

The fourth order symmetric SI is given by the following product of five $S_2$ operations:

$$S_4(\Delta t) = S_2(p_1\Delta t) S_2(p_2\Delta t) \cdots S_2(p_5\Delta t), \tag{23}$$

where $p_1,\ldots,p_5$ are

$$p_1 = p_2 = p_4 = p_5 = 1/(4 - 4^{1/3}),$$

$$p_3 = 1 - 4p_1. \tag{24}$$

Similarly, the sixth order symmetric SI is composed of 14 $S_2$ operations:

$$S_6(\Delta t) = S_2(p_1\Delta t) S_2(p_2\Delta t) \cdots S_2(p_{14}\Delta t), \tag{25}$$

where $p_i$ are

$$p_1 = p_2 = p_{13} = p_{14} = 0.392\,256\,805\,238\,773\,2,$$

$$p_3 = p_4 = p_{11} = p_{12} = 0.117\,786\,606\,679\,681\,0,$$

$$p_5 = p_6 = p_9 = p_{10} = -0.588\,399\,920\,894\,384,$$

$$p_7 = p_8 = 0.657\,593\,160\,341\,968\,4. \tag{26}$$

These and higher order SI are systematically derived via Lie algebraic formulation in Ref. [8].

#### *3. SI for time-dependent Hamiltonians*

We describe formulae of SI for time-dependent Hamiltonian $H(t)=A_1(t)+A_2(t)+\cdots+A_r(t)$, according to Ref. [8].

First, $S_2(\Delta t;t)$ is introduced as

$$S_2(\Delta t;t) \equiv e^{xA_1(t)/2}\, e^{xA_2(t)/2}\cdots e^{xA_{q-1}(t)/2} \times e^{xA_q(t)/2}\, e^{xA_{q-1}(t)/2}\cdots e^{xA_1(t)/2} \tag{27}$$

with $x=-i\Delta t/\hbar$, which can be interpreted as $\Delta t$ time step $SI_2$ operation with the virtual Hamiltonian with its parameter values fixed at the time $t$.

By using this, unitary time evolution $t$ to $t+dt$ with $H(t)$ is approximated by the $m$th order SI:

$$U_m(t+dt,t) = S_2(p_r\Delta t;t_r)\cdots S_2(p_2\Delta t;t_2)S(p_1\Delta t;t_1) \tag{28}$$

where $t_j=t+(p_1+p_2+\cdots+p_{j-1}+p_j)\Delta t$ and $p_j$ are the same as those of time-independent systems: (24) and (26) for fourth and sixth SIs, respectively.

We have seen that, even for time-dependent Hamiltonian, higher order SI are implemented by calling $SI_2$ subroutines several times [7,8], which reduces total programming cost essentially to that of $SI_2$ subroutine programming.

### B. Fock space truncation

For computing SI, we should truncate the infinite dimensional state space. A finite-dimensional, computational state space, which is suitable for low-energy dynamics description, is presented here.

We begin with splitting PIOS Hamiltonian into its diagonal and off-diagonal parts

$$H = H^D(\{n_j\}) + \lambda V^{\rm int}(\{a_j^\dagger, a_j\}),$$

$$H^D(\{n_j\}) = \sum_{j=1}^{N} \hbar\omega_j\left(n_j+\tfrac{1}{2}\right) + \sum_{\ell^0} W_{\ell^0,\ell^0}\prod :(n_j)^{\ell_j^0}:,$$

$$V^{\rm int}(\{a_j^\dagger, a_j\}) = \sum_{\ell^+\neq\ell^-} W_{\ell^+,\ell^-}\prod (a_j^\dagger)^{\ell_j^+}\,(a_j)^{\ell_j^-}, \tag{29}$$

where parameter $\lambda$ is introduced as the strength of off-diagonal coupling. The state space is the Fock space $\mathcal{F}$, spanned by the infinite-dimensional number states $\{|\{n_j\}\rangle; 0 \leqslant n_j < \infty\}$ of the $H^D$-eigen states.

With a cutoff parameter $E_{cut}$, an approximate, computational state space $\mathcal{F}_{\rm cut}$ is introduced by restricting its bases $|\{n_j\}\rangle$ with

$$H^D(\{n_j\}) \leqslant E_{\rm cut}. \tag{30}$$

To estimate $E_{\rm cut}$, let us consider the time-propagation with the initial condition $|\{n_j\}\rangle$. Substituting expansion with the eigen states $|E\rangle$ of the total Hamiltonian $|\{n_j\}\rangle=\Sigma_E\, C_E|E\rangle$ into

$$\langle\{n_j\}|(H-\langle H\rangle)^2|\{n_j\}\rangle = \lambda^2\langle\{n_j\}|(V^{\rm int})^2|\{n_j\}\rangle \tag{31}$$

leads to the relation:

$$\sum_E |C_E|^2(E-\langle E\rangle)^2 = \lambda^2\langle\{n_j\}|(V^{\rm int})^2|\{n_j\}\rangle, \tag{32}$$

which shows that probability $|C_E|^2$ has its mean $\langle E\rangle=\langle H^D\rangle=\langle H\rangle$ and the dispersion $\lambda\sqrt{\langle(V^{\rm int})^2\rangle}$. Hence, a number state $|\{n'\}\rangle$ that is excitable in the course of time satisfies $|H^D(\{n'\})-H^D(\{n\})| \simeq \lambda\sqrt{\langle(V^{\rm int})^2\rangle}$. For accurate computation, $\mathcal{F}_{\rm cut}$ must contain all excitable number states. Thus, $E_{\rm cut}$ should satisfy the following inequality:

$$H^D(n^0) + \lambda\sqrt{\langle(V^{\rm int})^2\rangle} < E_{\rm cut}. \tag{33}$$

Note that the dimension $L$ of $\mathcal{F}_{\rm cut}$ is roughly estimated to have the scaling $L\sim E_{\rm cut}^N/N!$, which is more efficient, compared to that of real-space grid truncation, $L\sim E_{\rm cut}^N$, which is used, for example, in SI-FFT method. This shows that our truncation scheme efficiently samples relevant states for multidimensional low-energy dynamics.

Note further that when the system has an additional symmetry, the computational state space can be divided into conserved subspaces associated with the symmetry. This reduces the size of dimension that must be treated at a computation. Translational invariance in $\phi^4$ MTRS model, for instance, conserves total momentum $P=\Sigma\hbar k_j n_j$ and each subspaces can be treated independently.

### C. Algorithm for computing SI

Having set the computational state space $\mathcal{F}_{cut}$, we now develop a numerical scheme for computing $SI_2$ in it. The development of $SI_2$ is sufficient for our purpose as discussed in Sec. III A. In this section, nonlinear parameter $\lambda$ is set to 1.

#### *1. Decomposition of $V_{int}$ into Hermitian binomials*

Elementary coupling operators, composed of conjugate terms

$$W_{\ell^+,\ell^-}\prod (a_j^\dagger)^{\ell_j^+}\,(a_j)^{\ell_j^-} + W^*_{\ell^+,\ell^-}\prod (a_j^\dagger)^{\ell_j^-}\,(a_j)^{\ell_j^+}, \tag{34}$$

are referred to as Hermitian binomials in this paper. The polynomial coupling $V^{\rm int}$ is the sum of a finite number of Hermitian binomials

$$V^{\rm int} = V^{\rm int}_{(1)} + V^{\rm int}_{(2)} + \cdots + V^{\rm int}_{(i)} + \cdots + V^{\rm int}_{(M)}, \tag{35}$$

$$V^{\rm int}_{(i)} = W_{\ell^+(i),\ell^-(i)}\prod (a_j^\dagger)^{\ell_j^+(i)}\,(a_j)^{\ell_j^-(i)} + W^*_{\ell^+(i),\ell^-(i)}\prod (a_j^\dagger)^{\ell_j^-(i)}\,(a_j)^{\ell_j^+(i)}, \tag{36}$$

where running numbers through the binomials ($i=1,2,\ldots,M$) are introduced.

Now we use Eq. (22) with

$$A_0 = H^D, \quad A_1 = V^{\rm int}_{(1)}, \quad A_2 = V^{\rm int}_{(2)}, \ldots, \quad A_M = V^{\rm int}_{(M)}, \tag{37}$$

which leads to an expression of $SI_2$:

$$\exp\left\{-i\frac{\Delta t}{\hbar}[H^D + V^{\rm int}_{(1)} + V^{\rm int}_{(2)} + \cdots + V^{\rm int}_{(M)}]\right\}$$
$$= e^{-i(\Delta t/2\hbar)V^{\rm int}_{(M)}} e^{-i(\Delta t/2\hbar)V^{\rm int}_{(M-1)}}$$
$$\times e^{-i(\Delta t/2\hbar)V^{\rm int}_{(M-2)}} \cdots e^{-i(\Delta t/2\hbar)V^{\rm int}_{(1)}} e^{-i(\Delta t/\hbar)H^D}$$
$$\times e^{-i(\Delta t/2\hbar)V^{\rm int}_{(1)}} \cdots e^{-i(\Delta t/2\hbar)V^{\rm int}_{(M-2)}} e^{-i(\Delta t/2\hbar)V^{\rm int}_{(M-1)}}$$
$$\times e^{-i(\Delta t/2\hbar)V^{\rm int}_{(M)}} + O(\Delta t^3). \quad (38)$$

Here the operation $\exp[-i(\Delta t/\hbar)H^D]|\mathbf{\Phi}\rangle$ is diagonal in the number base representation and thus is easy to compute. The remaining task is therefore developing a numerical scheme for evaluating exponential operations $\exp[-i(\Delta t/2\hbar)V^{\rm int}_{(i)}]|\mathbf{\Phi}\rangle$ for off-diagonal $V^{\rm int}_{(i)}$ $(i=1,2,\ldots,M)$.

#### 2. $V_{int}$ is block tridiagonal

Here we show that, with an appropriate ordering of number state bases, $V^{\rm int}_{(i)}$ is represented as a block tridiagonal matrix with zero diagonal elements. Without limiting the generality of the foregoing, we can write $V^{\rm int}_{(i)}$ as $V$ for notational simplicity.

We first introduce a counter $r$ that codes block matrices in $V$ with the initialization $r=1$. Operating $V$ on an arbitrary number state $|\mathbf{n}^r\rangle \equiv |\{n^r_j\}\rangle$ gives

$$V|\mathbf{n}^r\rangle = c^+[\mathbf{n}^r]|\mathbf{n}^r + \delta\mathbf{n}\rangle + c^-[\mathbf{n}^r]|\mathbf{n}^r - \delta\mathbf{n}\rangle, \quad (39)$$

where $\delta\mathbf{n} = \ell^+ - \ell^-$ and $c^{\pm}[\mathbf{n}^r]$ are nonzero matrix elements of $V$. By repeated application of $V$, a series of states is generated:

$$\{|\mathbf{n^r} + s_{\min}\delta\mathbf{n}\rangle, \ldots, |\mathbf{n^r} - \delta\mathbf{n}\rangle, |\mathbf{n^r}\rangle, \ldots, |\mathbf{n^r} + s_{\max}\delta\mathbf{n}\rangle\}, \quad (40)$$

where $s_{\max}$ and $s_{\min}$ are, respectively, the largest and smallest integers such that $|\mathbf{n}+s\delta\mathbf{n}\rangle \in \mathcal{F}_{cut}$. We write $s_{\max}-s_{\min}+1$ as $L_r$ and the $L_r$-dimensional subspace spanned by the series of states as $\mathcal{F}^r$.

With $|\mathbf{n}^r(s)\rangle \equiv |\mathbf{n}^r - (s-s_{\min}+1)\delta\mathbf{n}\rangle$, the projection operator $P_r$ onto $F^r$ is given by

$$P_r = \sum_{s=1}^{L_r} |\mathbf{n}^r(s)\rangle\langle\mathbf{n}^r(s)|. \quad (41)$$

$P_r$ satisfies

$$(1-P_r)VP_r = 0. \quad (42)$$

This shows that the operation of $V$ in $F^r$ is represented by a $L_r \times L_r$ matrix $B^r$, whose $(s,s')$th element $(B^r)_{s,s'}$ is given by $\langle\mathbf{n}^r(s)|V|\mathbf{n}^r(s')\rangle$. Moreover, from (39) only $(B^r)_{s,s+1}$ and $(B^r)_{s+1,s}$ for $s=1,\ldots,L_r-1$ are nonzero elements and thus $B^r$ is a tridiagonal matrix with zero diagonal elements.

Next we reset the counter $r \to r+1$, choose another number state that is not contained in $\mathcal{F}^1 + \ldots + \mathcal{F}^{r-1}$, and construct $(P_r, B^r)$ by the earlier procedure This is repeated until $\mathcal{F}^1 + \ldots + \mathcal{F}^r = \mathcal{F}_{cut}$ is fulfilled.

Finally, the total procedure generates $(P_r, B^r)$ for $r=1,2,\ldots,N_b$, where $N_b$ is the number of the block matrix $(\Sigma_{r=1}^{N_B} P_r = I)$. This shows that matrix representation of $V$ in the number bases can be permuted into the direct sum of $B^r$.

#### 3. Efficient operation of Hermitian binomial exponentials

Here continues the notation $V = V^{\rm int}_{(i)}$. With $B^r$, $|\mathbf{n}^r(s)\rangle$, and column vector $\mathbf{\Phi}^r$, $(\mathbf{\Phi}^r)_s \equiv \langle\mathbf{n}^r(s)|\mathbf{\Phi}\rangle, (s=1,\cdots,L_r)$, $e^{xV}|\mathbf{\Phi}\rangle$ is given by

$$e^{xV}|\mathbf{\Phi}\rangle = \sum_{r=1}^{N_b}\sum_{s=1}^{L_r} |\mathbf{n}^r(s)\rangle(e^{xB^r}\mathbf{\Phi}^r)_s, \quad (43)$$

where $x = -i\Delta t/(2\hbar)$.

We compute the coefficient vector $e^{xB^r}\mathbf{\Phi}^r$ by using a diagonal matrix with eigenvalues of $B_r$ and the associated diagonalizing matrix $S^r$, as

$$\mathbf{\Phi}^r := S_r\mathbf{\Phi}^r, \quad \mathbf{\Phi}^r := \exp(xD_r)\mathbf{\Phi}^r, \quad \mathbf{\Phi}^r := S_r^T\mathbf{\Phi}^r. \quad (44)$$

In order to efficiently compute (44), it is important to compute all linearly independent $D^r$ and store them beforehand in memory, because computing $D^r$ via general numerical schemes (such as, the QR method) require repeated matrix decompositions until the convergences and the computational efforts are much larger than those of matrix multiplications in (44), $\sim L_r^2$. Note that for matrices with $L_r \leqslant 5$, $D^r$ are not necessary to be stored, since their analytic expressions are obtained straightforwardly.

Then the required computation for (44) in runtime is as follows: $S^r$ is first generated with the computational effort $\sim L_r^2$ with use of $D^r$ and tridiagonality of $B^r$ and then matrix multiplications (44) are evaluated with $\sim L_r^2$.

Note that, since different blocks in (44) can be computable independently, the block diagonal matrix of $V[=V^{\rm int}_{(i)}]$ grants an inherent parallelism for the evaluation.

#### 4. Total $SI_2$ procedure and the computational cost

We here summarize our $SI_2$ procedure. Figure 1 shows the flowchart of one time step propagation, where "Union $D^r$" denotes storing in memory all linearly independent $D^r$ of $L_r \geqslant 6$ through $V^{\rm int}_{(i)}$ $(i=1,2,\ldots,M)$ and "$H^D$ evolution" operation of one time step propagation with diagonal Hamiltonian $H^D$.

Now we show that the computational cost for one time step $SI_2$ procedure depicted in Fig. 1 scales as $ML^{1+1/D}$, where $M$ is the number of binomials contained in $V^{\rm int}$ and $D$ is the effective dimension $N-I$ for $N$ degrees of freedom system with a number $I$ of conserved quantities. First, the average size of block matrices, $\langle L_r\rangle$, in $V^{\rm int}_{(i)}$ is approximately given by

$$\langle L_r\rangle = \sum_1^{N_b} L_r/N_b \sim L^{1/D} \quad (45)$$

and thus effective number of the average matrix is estimated by $\sim L/\langle L_r\rangle$. Hence, the average computational cost for $\exp(V^{\rm int}_{(i)})|\mathbf{\Phi}\rangle$ via Eq. (44), is approximately estimated to be

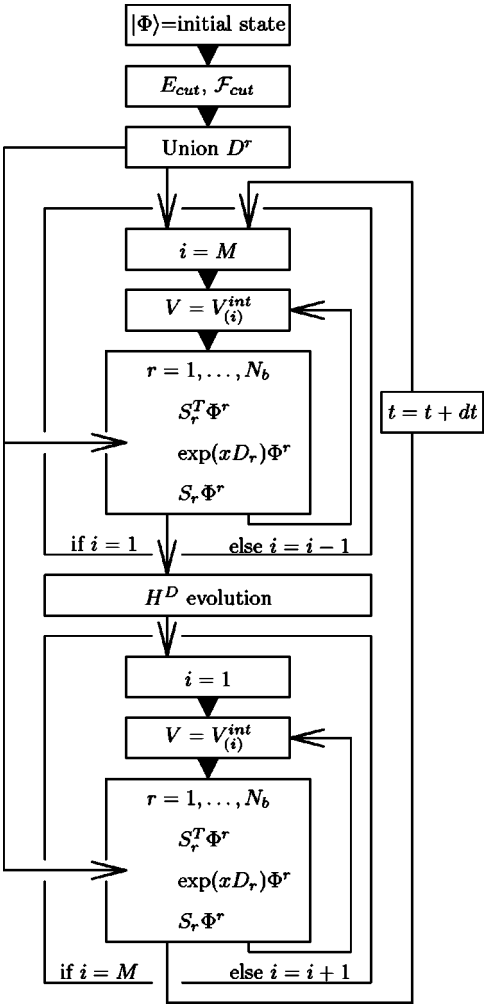


FIG. 1. Total procedure of $SI_2$. $N_b$ is the number of block matrices in $V=V^{\text{int}}_{(i)}$. See Eq. (44) for operations $S^T_r\Phi^r$, $\exp(xD_r)$, and $S_r\Phi^r$, where $x=-i\Delta t/(2\hbar)$.

$$\frac{L}{\langle L_r\rangle}\langle L_r\rangle^2 \sim \frac{L}{L^{1/D}}(L^{1/D})^2 = L^{1+1/D}. \tag{46}$$

Thus, the total computational cost required for the $SI_2$ in Fig. 1 is $ML^{1+1/D}$ [= Eq. (46) times $M$].

Note that our numerical time propagation scheme presented here is effective, compared to the other naïve schemes. For example, the time propagation schemes via diagonalization of total Hamiltonian typically cost at $\sim L^3$. This efficiency is because SI is decomposed into small size matrix multiplications whose dimensions are much less than state space dimension $L$.

## IV. NUMERICAL RESULT: THE ACCURACY AND CONVERGENCE

In this section, we show the accuracy of our method developed in the previous section, using $\phi^4$ MTRS with $\lambda=1$ introduced in Sec. II.

Recall that we have introduced two approximations into our method: one is the time step $dt$ and the other is the energy cutoff $E_{\text{cut}}$ to introduce computational state space $\mathcal{F}_{\text{cut}}$. Our scheme should then satisfy the following convergences: (1) With a fixed $E_{\text{cut}}$, $m$th order SI converges with $O(dt^m)$ accuracy as $dt\to 0$; and (2) After this $dt\to 0$ limit, the wave function that is accurate in $\mathcal{F}$ is given by taking the limit of $E_{\text{cut}}\to\infty$.

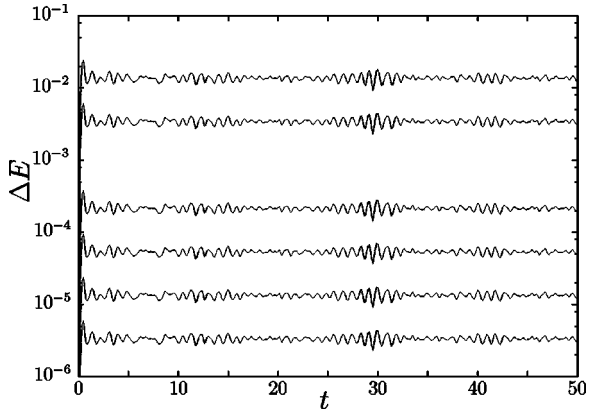


FIG. 2. $\Delta E$ as a function of time $t$. From the top $dt=2^{-4},2^{-5},2^{-6},2^{-7},2^{-8},2^{-9}$. Fitting $\Delta E$ of $dt\leqslant 2^{-6}$ with Eq. (48) gives $m\simeq 2$. Eq. (48) is similarly confirmed up to sixth order SI.

### A. The *dt* convergence

By using our method under $E_{\text{cut}}=32$ with various time steps $dt$, wave functions are computed. The initial state is a normalized state in $\mathcal{F}_{\text{cut}}$, whose probabilities for the number states are random numbers from a uniform distribution and the phases are random numbers from the uniform distribution in $[0,2\pi)$. Now we study the consistency of our method with the following three indicators of accuracy: energy fluctuation $\Delta E$; difference to the exact wave function, $d_1$; change caused by replacement of $dt$ with $dt/2$, $d_2$.

#### *1. Energy fluctuation*

Since all the parameters included in this $\phi^4$ MTRS Hamiltonian ($\lambda=1$) are constant, the expectation value for the total energy is conserved. Hence, we measure the accuracy of our method, by the energy deviation from the initial expectation value

$$\Delta E = \left|\langle t;\mathrm{SI}_m,dt|H|t;\mathrm{SI}_m,dt\rangle - \langle t=0|H|t=0\rangle\right|, \tag{47}$$

where $|t=0\rangle$ denotes the initial wave function and $|t;\mathrm{SI}_m,dt\rangle$ the wave function at a time $t$ computed via $m$th order SI with $dt$ timestep.

Figure 2 plots $\Delta E$ against $t$, for $\phi^4$ MTRS with three degrees of freedom ($N=3$), where second order schemes are used with $dt=2^{-4},2^{-5},2^{-6},2^{-7},2^{-8},2^{-9}$. This shows that after the transient increase, each $\Delta E$ remains nearly constant, with small fluctuations around the average. As $dt$ approaches zero, $\Delta E$ approaches zero consistently with the order of SI, $m$, for sufficiently small $dt$:

$$\Delta E \simeq A(dt)^m, \tag{48}$$

where $A$ is a constant depending on $m$.

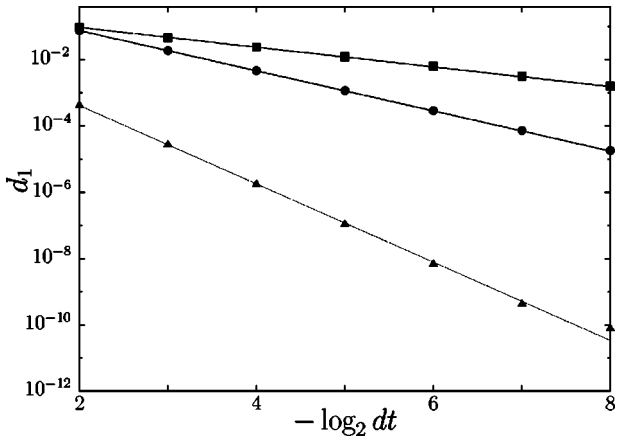


FIG. 3. Logarithmic plot of $d_1$ of first, second, and fourth order SI with time $t=50$ against $dt$. Symbols ■, ●, and ▲ are results of first, second, and fourth order SI, respectively. The solid lines are fitting functions $d_1=A_m dt^m$ via fitting parameters $A_m$ for $m=1,2,4$.

We have thus numerically confirmed that energy conservation is recovered in the $dt\to 0$ limit, consistently with the order of SI. The accuracy of the other observables is, however, not yet clarified. To elucidate this, we should proceed to study the accuracy of the wave functions.

#### *2. Difference from the exact wave function*

We use the difference $d_1$ between $|t;\mathrm{SI}_m,dt\rangle$ and the exact wave function $|t;\mathrm{exact}\rangle$, as an indicator for the accuracy of wave function

$$d_1 = \| |t;\mathrm{exact}\rangle - |t;\mathrm{SI}_m,dt\rangle \|, \tag{49}$$

where vector norm $\| |f\rangle \|$ is defined by $\sqrt{\langle f|f\rangle}$. For a time $t=Ndt$, $m$th order SI has

$$U(t) = [S_m(x)]^N + tO(dt^m), \tag{50}$$

where $U(t)=U(dt)^N$ and $U(dt)=S_m(x)+O(dt^{m+1})$ are used. Multiplying both sides of Eq. (50) by $|t=0\rangle$ leads

$$|t;\mathrm{exact}\rangle = |t;\mathrm{SI}_m,dt\rangle + tO(dt^m). \tag{51}$$

From this, for a fixed $t$, $d_1$ depends on $dt$ as follows:

$$d_1 \sim O(dt^m). \tag{52}$$

To confirm Eq. (52) numerically, we compute $|t;\mathrm{SI}_m,dt\rangle$ by applying our first, second, and fourth order method to $\phi^4$ MTRS with three degrees of freedom ($N=3$), while $|t;\mathrm{exact}\rangle$ is given by

$$|t;\mathrm{exact}\rangle = \sum_E |E\rangle\, e^{-i(E/\hbar)t}\langle E|t=0\rangle, \tag{53}$$

where eigenenergy $E$ and the associated eigenstate $|E\rangle$ are computed via numerical diagonalization of Hamiltonian matrix.

Figure 3 plots $d_1$ at $t=50$ as a function of $dt$. This shows that all orders of our scheme converge to the exact integrator as $dt$ approaches zero. In addition, the theoretical estimation of Eq. (52) is numerically reproduced. These show the actual utility of our numerical method.

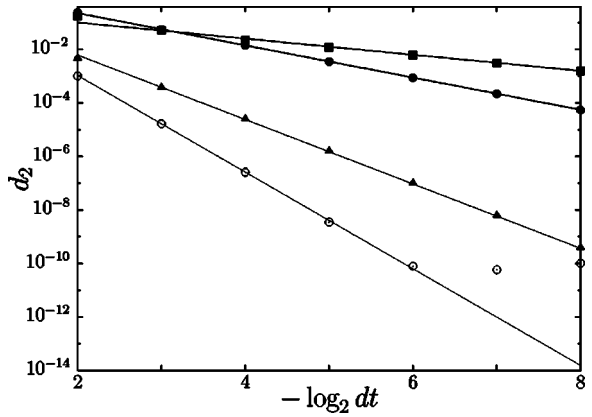


FIG. 4. $d_2$ of $\phi^4$ MTRS with three degrees of freedom as a function of $dt$. Symbols ■, ●, ▲, and ○ are results of first, second, fourth, and sixth order SI, respectively. The solid lines are fitting functions $d_2=A_m dt^m$ via fitting parameters $A_m$ for $m=1,2,4,6$.

We have confirmed the usefulness of our method in $\phi^4$ MTRS with *three* degrees of freedom. However, $d_1$ is hard to compute in systems with more than three degrees of freedom, because diagonalization of Hamiltonian matrix in Eq. (52) becomes difficult in such a high dimensional system.

#### *3. Change of wave function induced by $dt\to dt/2$*

To study the accuracy of our method in more degrees of freedom systems, we introduce the following indicator:

$$d_2 = \left\| |t,\mathrm{SI}_m,dt\rangle - \left| t,\mathrm{SI}_m,\frac{dt}{2}\right\rangle \right\|. \tag{54}$$

This measures the change of wave function induced at time $t$, by the replacement of $dt\to dt/2$. At a fixed time $t$, $d_2$ depends on $dt$ as

$$d_2 = O(dt^m - (dt/2)^m) = O(dt^m), \tag{55}$$

which is easily derived from Eq. (51).

Let us first confirm Eq. (55) through the numerical results of $\phi^4$ MTRS with three degrees of freedom. Figure 4 plots $d_2$ at $t=50$, against $dt$. The $dt$-dependency (55) is clearly seen from first, second, fourth, and sixth order SI results in the figure, although sixth order SI results stop decreasing at $d_2 \sim 10^{-10}$, because of the round-off error.

Having confirmed the usefulness of the indicator $d_2$, we now apply this consideration to the higher dimensional systems. In Fig. 5, $d_2$ of second order SI for $\phi^4$ MTRS with five, and seven degrees of freedom are plotted against time step $dt$, which shows clear $dt$-dependence (55). In addition, we have confirmed the dependence (55) for the higher order SI ($m=4,6$) in the same way.

In this subsection, we have numerically confirmed that our scheme, with a fixed computational Fock space, converges to the accurate result as time step $dt\to 0$, for multidimensional systems with up to seven degrees of freedom, where the convergences are consistent with the SI orders.

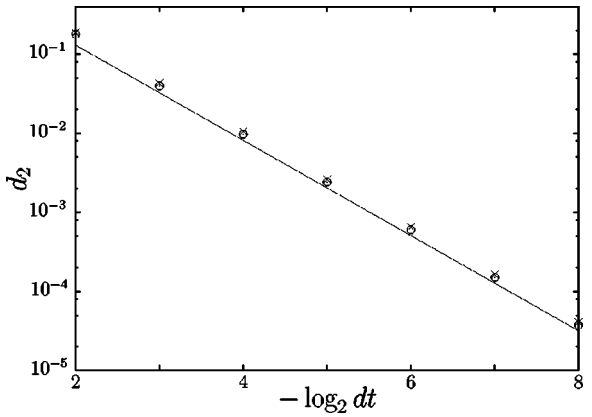


FIG. 5. Plot of $d_2$ for five, seven degrees of freedom $\phi^4$ MTRS with second order SI ($m=2$), against $dt$. Symbols $\times$ and $\bigcirc$ are for five and seven degrees of freedom, respectively. The solid line is $\sim dt^2$ for eye guidance.

### B. The $E_{\mathrm{cut}}$ convergence

We now confirm that computed wave functions with our method approach correct wave functions in $\mathcal{F}$, in the limit of cutoff parameter $E_{\mathrm{cut}}\to\infty$ ($\mathcal{F}_{\mathrm{cut}}\to\mathcal{F}$).

To check this, we introduce an indicator, $d_3$, that shows acquiring accuracy of wave function in $\mathcal{F}$, by approaching zero. First, note that, as we saw in the previous subsection, an approximate wave function, $|t;\epsilon,E_{\mathrm{cut}}\rangle$, in $\mathcal{F}_{\mathrm{cut}}$ with $\epsilon$ accuracy is computable by using any SI wave function $|t;\mathrm{SI}_m,dt,E_{\mathrm{cut}}\rangle$, which satisfies the following inequality:

$$\| \, |t;\mathrm{SI}_m,dt,E_{\mathrm{cut}}\rangle - |t;\mathrm{exact},E_{\mathrm{cut}}\rangle \| \leqslant \epsilon, \tag{56}$$

where arguments $E_{\mathrm{cut}}$ are appended to specify the computational state state. Then, by using $|t;\epsilon,E_{\mathrm{cut}}\rangle$, an indicator $d_3$ is introduced as

$$d_3 = \| \, |t;\epsilon,E_{\mathrm{cut}}\rangle - |t;\epsilon,E_{\mathrm{cut}}+1\,\rangle \|. \tag{57}$$

Namely, when $d_3\leqslant\epsilon$ are satisfied for sufficiently large $E_{\mathrm{cut}}$, then this guarantees the acquisition of a wave function in $\mathcal{F}$ with $\epsilon$-order accuracy

Let us numerically confirm this inequality. Figure 6 shows $d_3$ of $\phi^4$ MTRS with three degrees of freedom, against $E_{\mathrm{cut}}$.

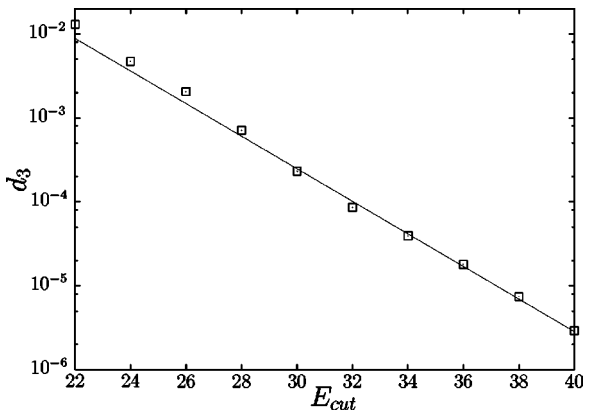


FIG. 6. $d_3$ vs $E_{\mathrm{cut}}$. The solid line is a fitted function $\exp(a+bx)$ with $a=5.09, b=-0.45$.

The initial state has expansion coefficients that are uniformly distributed around $H_0(\{n_j\})\sim 10$ and $\epsilon$ is set as $10^{-5}$. This clearly shows that $d_3$ exponentially converges as $E_{\mathrm{cut}}\to\infty$. Additionally, we have confrmed that, regardless of the details of initial states, $d_3$ exponentially converges to zero even when $\phi^4$ MTRS have five seven degrees of freedoms.

In this section, we have numerically confirmed that our scheme exponentially converges to the accurate time evolution in the limit of $\mathcal{F}_{\mathrm{cut}}\to\mathcal{F}$, for $\phi^4$ MTRS with up to seven degrees of freedom. Even for other systems, $d_3$ are expected to converge at $E_{\mathrm{cut}}\to\infty$, only if they classically have bounded equienergy surfaces in phase spaces at arbitrary total energies. The convergence would depend on the details of the system. For example, it could differ from exponential convergence.

## V. CONCLUSION AND REMARK

In this paper, we have presented a method for computing quantum dynamics of PIOS. This model provides a basis of crosscutting analysis for multidimensional low-energy dynamics from paradigmatic dynamical models, such as FPU-$\beta$ and lattice $\phi^4$, to physical systems, such as intramolecular vibration redistribution and Bose-Einstein condensation. We have presented details of renormalization procedure for a PIOS model, $\phi^4$ MTRS.

Our method is based on the SI scheme, and thus preserves time reversal symmetry and unitarity. Furthermore, it has a practical advantage that higher order SI is easily implemented by several calls of $\mathrm{SI}_2$ subroutines. This advantage is available even for the time-dependent Hamiltonian system, which is notable because this property is indispensable, especially for analysis of physical systems under external strong fields and/or random perturbations.

In order to effectively evaluate the SI, our method takes advantage of the block tridiagonality of binomial terms in the polynomial interaction. The computational cost for one step $\mathrm{SI}_2$ is $\sim L^{1+1/D}$ with the truncated space dimension $L$ and effective dimension $D$. This method is more efficient for multidimensional systems, compared to the existing method, such as diagonalization method of Hamiltonian matrix and SI-FFT method. Furthermore, this procedure grants an inherent parallelism.

In the last section, the accuracy of our method is illustrated by removing two cutoffs, time step size $dt$ and truncation $\mathcal{F}_{\mathrm{cut}}$ of Fock space $\mathcal{F}$. We have confirmed the convergence below: (1) For a fixed $\mathcal{F}_{\mathrm{cut}}$, an error of wave function converges as $dt\to 0$, consistently with the order of SI. (2) The computed wave function, accurate in $\mathcal{F}_{\mathrm{cut}}$, converges to the correct wave function in $\mathcal{F}$, as $\mathcal{F}_{\mathrm{cut}}$ approaches $\mathcal{F}$. These show that we have actually constructed an accurate numerical scheme for computing quantal dynamics of multidimensional PIOS models.

Finally, we here add a remark on the applicability of our method on eigenvalue problem. Repeated operation of $f(H)=H\exp(-\beta H)$ makes any state vector converge to the eigenstate that has an eigenenergy nearest to energy $1/\beta$, for a Hamiltonian $H$ with nonnegative eigenenergy. Note that operation $\exp(-\beta H)$ is efficiently computable by using our

time-propagation method with replacement of time with imaginary time. We have thus obtained a numerical scheme for eigenvalue problem that enables us to compute the eigen state with an eigenenergy adjacent to an arbitrary energy. For (quasi-)degenerate eigenenergy systems, standard techniques, such as the Rayleigh-Ritz method [17], would be useful to accelerate the convergence. We further expect that our method is directly applicable for recently developed, sophisticated time-domain approaches to calculate various physical quantities [18,19]. We hope that this method will improve our understandings of multidimensional quantal dynamics.

## ACKNOWLEDGMENTS

The author is grateful to A. Shudo and A. Tanaka for their enlightening discussions and continuous encouragement.

[1] For a review see, e.g., J. Weiner, V. S. Bagnato, S. Zilio, and P. S. Julienne, Rev. Mod. Phys. **71**, 1 (1999); A. J. Legget, *ibid.* **73**, 307 (2001).
[2] K. Yamanouchi, N. Ikeda, S. Tsuchiya, D. M. Jonas, J. K. Lundberg, G. W. Adamson, and R. W. Field, J. Chem. Phys. **95**, 6330 (1991).
[3] E. R. Lovejoy, S. K. Kim, and C. B. Moore, Science **256**, 1541 (1992); S. K. Kim, E. R. Lovejoy, and C. B. Moore, J. Chem. Phys. **102**, 3202 (1995).
[4] A. Nauts and R. E. Wyatt, Phys. Rev. Lett. **51**, 2238 (1983).
[5] R. Kosloff, J. Phys. Chem. **92**, 2087 (1988).
[6] H. Tal-Ezer and R. Kosloff, J. Phys. Chem. **81**, 3967 (1984).
[7] H. Yoshida, Phys. Lett. A **150**, 262 (1990).
[8] M. Suzuki, Proc. Jpn. Acad., Ser. B: Phys. Biol. Sci. **69**, 161 (1993).
[9] N. Watanabe and M. Tsukada, Phys. Rev. E **62**, 2914 (2000).
[10] K. Takahashi and K. Ikeda, J. Chem. Phys. **99**, 8680 (1993).
[11] T. Uzer and W. H. Miller, Phys. Rep. **199**, 73 (1991).
[12] M. Toda, Adv. Chem. Phys. **123**, 153 (2002).
[13] E. V. Shuryak, Zh. Eksp. Teor. Fiz. **71**, 2039 (1976) [Sov. Phys. JETP **44**, 1070 (1976)].
[14] K. Huang, *Statistical Mechanics*, 2nd ed. (Wiley, New York, 1987).
[15] For a review see, e.g., B. V. Chirikov, Phys. Rep. **52**, 263 (1979); G. Zaslavsky, R. Z. Sagdeev, D. A. Usikov, and A. A. Chernikov, *Weak Chaos and Quasiregular Patterns* (Cambridge University Press, Cambridge, 1991); A. J. Lichtenberg and M. A. Lieberman, *Regular and Stochastic Motion* (Springer-Verlag, New York, 1983).
[16] For systems with more than one spatial dimension, the renormalization of nonlinear parameter $\lambda$ are also required.
[17] G. H. Golub and C. F. Van Loan, *Matrix Computations*, 3rd ed. (Johns Hopkins Press, Baltimore, 1996).
[18] K. Takatsuka and N. Hashimoto, J. Chem. Phys. **103**, 6057 (1995).
[19] T. Iitaka and T. Ebisuzaki, Phys. Rev. Lett. **90**, 047203 (2003).